Title: Elytra coupling of the ladybird *Coccinella septempunctata* functions as an energy absorber in intentional falls

Authors: Jie Zhang [1], Qiufeng Yuan [2], Yiling Jiang [1], Hong Pang [3], Hamed Rajabi [4], Zhigang Wu [1,] *, Jianing Wu [1,] *

Affiliations:

1. School of Aeronautics and Astronautics, Sun Yat-Sen University, Guangzhou, 510006, P. R. China
2. School of Engineering and Technology, China University of Geosciences, Beijing, 100191, P. R. China
3. School of Ecology, Sun Yat-Sen University, Guangzhou, 510006, P. R. China
4. Division of Mechanical Engineering and Design, School of Engineering, London South Bank University, London, UK

*Corresponding author E-mail:

wuzhigang@mail.sysu.edu.cn (Zhigang Wu)

wujn27@mail.sysu.edu.cn (Jianing Wu)

Abstract:

Some insects, such as bees, wasps, and bugs, have specialized coupling structures to synchronize the wing motions in flight. Some others, such as ladybirds, are equipped with coupling structures that work only at rest. By locking elytra into each other, such structures provide hindwings with a protective cover to prevent contamination. Here, we show that the coupling may play another significant role: contributing to energy absorption in falls, thereby protecting the abdomen against mechanical damage. In this combined experimental, numerical and theoretical study, we investigated free falls of ladybirds (*Coccinella septempunctata*), and discovered that upon collision to the ground, the coupling may fail and the elytra may unlock. This unlocking of the coupling increased the energy absorption by 33%, in comparison to when the elytra remain coupled. Using micro-CT scanning, we developed comparative models that enabled us to simulate impact scenarios numerically. Our results showed that unlocking of the coupling, here called elytra splitting, reduces both the peak impact force and rebound velocity. We fabricated the insect-inspired coupling mechanism using 3D printing and demonstrated its application as a damage prevention system for quadcopters in accidental collisions.

Keyword: ladybird, elytra coupling, landing, energy absorption.

1. Introduction

The performance of energy absorbing structures in vertebrates, such as turtle shells *Terrapene carolina* (Rhee *et al.*, 2009; Wu *et al.*, 2017), sheep horns *Ovis canadensis* (Fuller and Donahue, 2021), and woodpecker beaks *Melanerpes carolinus* (Lee *et al.*, 2014), has fascinated researchers for many decades (Tarakanova and Buehler, 2012). For instance, woodpeckers perform repeated strikes at a speed of 6-7 m/s while pecking for food, resulting in an impact deceleration of the order of 1000 g (May *et al.*, 1979). Horns of bighorn sheep, as another example, resist forces of up to 3400 N during fights (Trim *et al.*, 2011). The massive impact loads experienced by such biological structures and the absence of any catastrophic failure, suggest that they have undergo adaptations

to excessive impact stresses (Drake *et al.*, 2016). Similar to vertebrates, energy absorbing structures play an important role in the survival of invertebrates. Orb webs of the spider *Argiope aurantia*, which captures insects in midflight, can absorb prey kinetic energy without breaking (Foelix, 2011; Sensenig *et al.*, 2012). Shells of the mantis *Odontodactylus scyllarus* withstand thousands of high-velocity blows that the animal delivers to its prey (Grunenfelder *et al.*, 2014). The leg muscles of the cockroach *Blaberus discoidalis* not only generate the power for locomotion, but operate as active dampers that absorb energy during running (Full *et al.*, 1998).

Beetles, one of the most diverse orders of insects with about 400 thousand species, represent striking examples of energy absorbing structures (Phan and Park, 2020). Their elytra, which are in fact hardened forewings, are ventrally jointed to the body. By keeping the elytra closed, coupling structures enable the beetles to pass through restricted environments without damaging the abdomen or hindwings (Dai and Yang, 2010; Breed and Ball, 1908; Dai *et al.*, 2008; Frantsevich *et al.*, 2005). Furthermore, when disturbed by predators, such as birds, amphibians, and reptiles, beetles play dead and fall to the ground. During this displaying behavior, the elytra show a high energy absorption capacity (Zhang *et al.*, 2021; Burgio, 2013).

Knowing the internal morphology and material properties of elytra can provide insights for the development of novel energy absorbing structures (Hao and Du, 2018), a reason that has sparked research attention to the biomechanical properties of beetle elytra (Sun and Bhushan, 2012). Previous studies have shown that beetle elytra are layered structures, primarily made of chitin microfibrils and protein (Jalali and Heshmati, 2016; Tasdemirci *et al.*, 2015), and consist of a dorsal and a ventral layer that are interconnected by columnar trabecula (Kundanati *et al.*, 2018; Hadley, 1986). With the support of these structures and existing cavities, the elytra provide high strength and efficient energy absorption that prevent damage (Hong *et al.*, 2003; Gunderson and Schiavone, 1995). Previous research, however, has fully neglected the potential role of the coupling structure in the energy absorption properties of the elytra. To understand whether this might be the case, here we investigated the falling dynamics of the ladybird *Coccinella septempunctata* and found that, while landing on the elytra, the coupling

structures can provide energy absorption and reduce both the rebound height and velocity after collision. We further show that the elytra coupling can offer novel insect-inspired designs for mitigating body injuries as well as other applications that involve collisions.

2. Materials and Methods

2.1. Speciments

Ladybirds (*C. septempunctata*) were collected from Zhengzhou, Henan Province, China (34.16°N, 112.42°E), and kept in a terrarium filled with indoor horse bean seedlings (*Vicia faba L.*) in our laboratory in Guangzhou, Guangdong Province, China (23.13°N, 113.27°E) at 26℃ and 60% humidity with controlled day-night cycle (12h/12h) (figure 1(a)). All ladybirds were fed with aphids (*Megoura japonica*) living on the horse bean seedlings (Frazer and Gilbert, 1976; Zhang *et al.*, 2021). For the experiments, we randomly selected twenty ladybirds and recorded their body masses m. The length a, width b, and height c of each sample were measured using vernier calipers (AIRAJ 1331, AIRAJ, USA) (figure 1(b)).

2.2. Calculation of energy absorption in falls

To measure the energy absorption during impacts, we dropped the insects (no initial velocity) onto a hard surface through a transparent cylindrical tube (50 cm in length and 4.5 cm in diameter) to eliminate the potential effect of the surrounding air (figure 1(c)). To describe the orientation of the ladybirds, we set up a coordinate system at the center of the abdominal plane o. The x axis pointed from point o towards the head, and the z axis coincided with the normal direction of the abdomen. The y axis was determined by the right-hand rule. The motion of the falling ladybirds was quantified by roll, pitch, and yaw angles, about the axes x, y, and z, respectively. Two high-speed cameras (Phantom, VEO-E 310L, USA), equipped with micro-lenses (Canon, EF100mmf/2.8LISUSM, Japan), were used to record the falling ladybirds at 1000 fps. The first high-speed camera (Camera #1) was used to observe the deformation of the elytra at the impact. Using the second high-speed camera (Camera #2), we analyzed the

dynamics of falling, landing, and rebound before and after the impact, including the heights (h_1: before impact; h_2: after impact), translational velocities (v_1: before impact; v_2: after impact), and angular velocities (ω_1: before impact; ω_2: before impact) of the specimens.

Mechanical energy E_i of an object of mass m, height h, translational velocity v, and angular velocity ω can be obtained using the below equation:

$$E_i = mgh_i + \frac{1}{2}\left(mv_i^2 + J\omega_i^2\right) \tag{1}$$

where, J is rotational inertia. The index i is the sequence of the record; i=1 represents the initiation of the fall, and i=2 is when the rebound after collision with the ground has taken place.

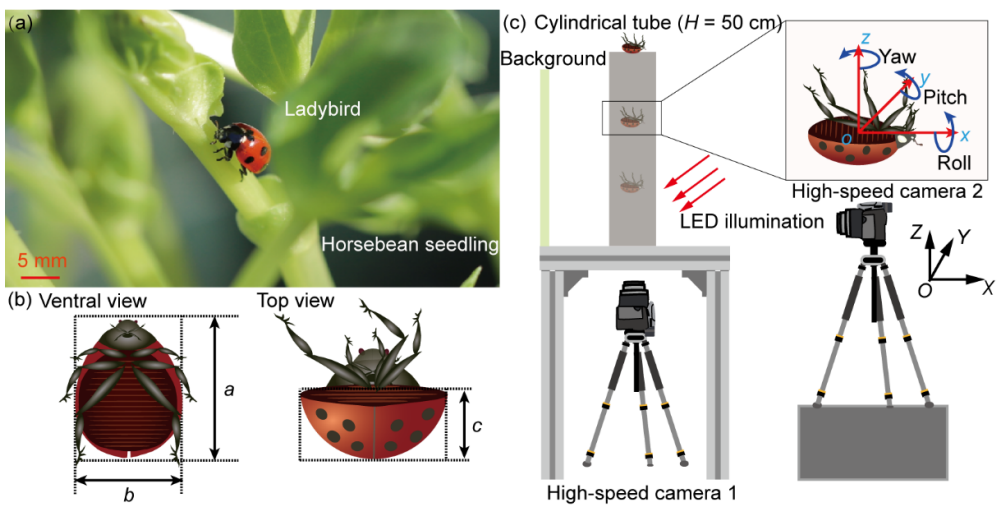

Figure 1. Experimental setups for fall tests. (a) Ladybirds were kept in a terrarium filled with horse bean seedlings. (b) Measured dimensions of a ladybird body. (c) High-speed filming for the analysis of the falls and collisions of ladybirds. The defined *o-xyz* coordinates is shown here.

2.3. Impact force measurement

We built an experimental set-up with a force plate (HE6X6, AMTI, USA) to measure the impact force of ladybirds in free falls (figure 2(a)). The resolution of this force plate is 8.8 mN. To eliminate the influence of airflows and external vibrations on the measurements, we designed a screen shield made up of acrylic sheet around the force plate, and placed a foam board under the force plate. The sampling frequency and duration of the force plate were set as 100 Hz and 10 s, respectively. Additionally, a

decibel meter was placed next to the force plate to measure the noise from the impacts. For experiments, we dropped the ladybirds (n = 20) from a constant height of 50 cm on the force plate with no initial velocity. This height corresponds to the average height of the plants on which ladybirds were observed.

2.4. Scanning electron microscopy

Scanning electron microscopy (SEM) was used to examine the microstructure of the coupling between the elytra of the ladybirds. The fresh samples of elytra (n = 3) were fixed by soaking in 2.50% glutaraldehyde for 3 h at 26℃. The samples were then cleaned with 0.10 mol/L phosphate buffer (pH = 7) for 20 minutes, and dehydrated though an ascending ethanol series (at 75%, 80%, 85%, 90%, 95%, and 100% for 12 h) before freeze drying. The samples were mounted on SEM stubs with graphite adhesive tape. Coated in gold palladium, and observed under a SEM (FEI Quanta 200, Czech Republic) in high-vacuum mode at 15 kV.

2.5. Atomic force microscopy

Atomic force microscopy (AFM) was used to characterize the stiffness of the ladybird elytra. For this purpose, we used a Dimension Icon AFM (FastScan, BRUKER, USA) (figure 2(b)) equipped with a probe (RTESPA-150, BRUKER, USA). Small pieces (~ 1 mm × 1mm) were cut from the fresh elytra as specimens and covered by wet cotton to prevent dehydration. We tested the specimens (n = 3) at ten sampling points along the length of each specimen. In the peak force tapping mode, the vibrating tip performed vertical indentation to record force curves for each sampling point on the surface of the specimens. By real-time analysis of the force curves, the Young's modulus of the specimens at each sampling point was obtained using the Derjaguin, Muller, Toporov (DMT) model (Li *et al.*, 2019).

2.6. Micro-computed tomography

The dynamic X-ray micro-computed tomography (micro-CT) system from Shanghai Synchrotron Radiation Facility (SSRF) was employed to reconstruct the three-dimensional (3D) shape of the elytra of ladybirds (figure 2(c)). The beamline BL13W1 with 8.0 keV to 72.5 keV and several sets of X-ray imaging detectors with

varying pixel sizes (0.19 μm-24 μm) were used to realize X-ray micro-CT in-line imaging (Wang *et al.*, 2020). In this experiment, the photon energy and pixel size were set as 15 keV and 3.25 μm, respectively (Shang *et al.*, 2020; Xie *et al.*, 2020). A ladybird specimen, placed in a plastic tube, was mounted on the beamline positioner. After imaging, we processed the obtained images using the PITRE and Mimics software (Materialise, Belgium) for phase-sensitive X-ray image processing and tomography reconstruction to generate the 3D models of the elytra (Chen *et al.*, 2012).

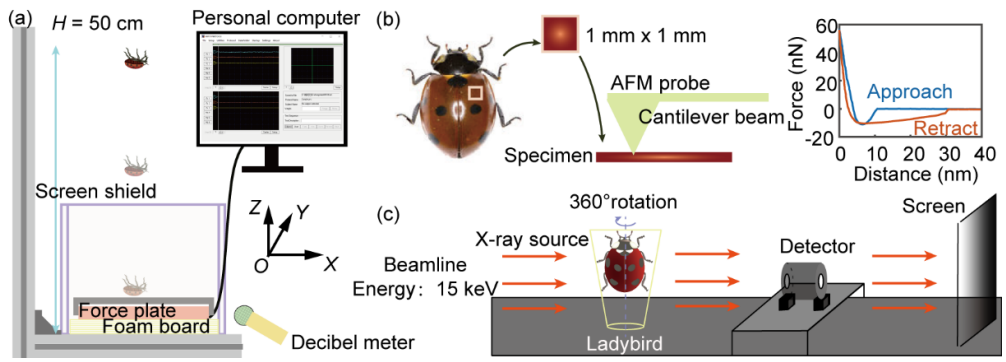

Figure 2. Schematic diagram of experimental testing and imaging platform. (a) Diagram of impact force measurement platform. (b) Schematic diagram of the atomic force microscopy. (c) Schematic of the micro-computed tomography.

2.7. Finite element modeling

Considering that the anterior parts of the elytra were always locked under the impact, we focused on the posterior parts (x<0) and defined two comparative models, namely continuum and split models. We used our models to uncover how the coupling can influence the energy absorption by the elytra in impacts. The first model was a continuum shell that was geometrically similar to the profiles obtained from micro-CT scans. This model was used to simulate the state at which the elytra are tightly coupled with each other under the impact. By contrast, the second model consisted of two halves of shells coupled with each other by a coupling that can be split under the impact.

For the dynamics of the models in falls, the governing equations were deployed, including equilibrium equation $\sigma_{ij,j} + f_i = 0$, geometric equation $\varepsilon_{i,j} = \left(u_{i,j} + u_{j,i}\right)/2$, and constitutive equation $\sigma_{ij} = \lambda\varepsilon_{kk}\delta_{ij} + 2G\varepsilon_{ij}$, in which $\lambda = \dfrac{E\nu}{(1+\nu)(1-2\nu)}$, and

$G=\frac{E}{1+v}$. Here, E and v represented elasticity modulus and Poisson's ratio, respectively.

Based on the Hamilton variational principle, the governing equations for dynamic collisions can be obtained (Hien and Kleiber, 1990).

$$M_i\ddot{U}+C_i\dot{U}+K_iU=0 \tag{2}$$

where, M_i was the mass matrix, C_i was the damping matrix, K_i was the stiffness matrix. Here, $\ddot{U}$, $\dot{U}$, and U were the acceleration, velocity and displacement vectors, respectively.

From the statistical analysis of the recorded videos of the ladybirds in falls, we found that different parts of the elytra might come in contact with the ground. This may result in different energy absorption capacities. To include the effect of this in our models, we defined the landing region by the landing angle, which is acute angle between the plane *xoy* and the ground. Here, we set three representative landing angles of 0°, 30°, and 60°, respectively. We also used the material properties of the models as shown in Table 1 (Rivera *et al.*, 2020).

Table 1. The material properties of the models

Elasticity modulus (GPa)	Poisson's ratio	Density (kg/m^3)	Initial velocity (m/s)
3	0.3	500	2.75

During collisions, both models can absorb energy through the elastic deformation, which convert the energy into the internal energy E_{in}. The internal energy of the models could be written as:

$$E_{\text{in}}=\sum_{i=1}^{n}\int_{v_i} f\left(\varepsilon_i\right)dv_i \tag{3}$$

where, $f\left(\varepsilon_i\right)$ and v_i are the strain energy density and the volume of an element of the model, and n is the total number of elements.

3. Results and discussion

3.1. Energy absorption in falls

The ladybirds (*C. septempunctata*, m = 27.04 ± 6.62 mg, n = 20) that were falling from a height of 50 cm could adjust their orientations during falling, enabling them to land on the elytra in 80% of the cases, regardless of the initial orientation. In all events, we could measure the sound of 60-70 dB caused by the collision of the elytra to the ground. This sound, which is analogous to the noise generated by a car running at 65 km/h, may reflect the intensity of the collisions (Behzad *et al.*, 2007). However, the ladybirds were not crashed to death by the impact force, which may suggest the presence of an energy absorbing mechanism within the elytra. Considering that the part at which the elytra collide to the ground may affect the energy absorption, we divided the semi-ellipsoidal shell (an average length of a = 7.08 ± 6.62 mm, width of b = 5.25 ± 0.49 mm, and height of c = 3.14 ± 0.54 mm) formed by the two elytra into a projected circle. We subdivided the projected circle into three ring-like regions, namely the inner, central, and outer rings, to quantify the landing region (figure 3). The inner, central, and outer rings are in concordance with the landing angles of 0°-30°, 30°-60°, 60°-90°, respectively.

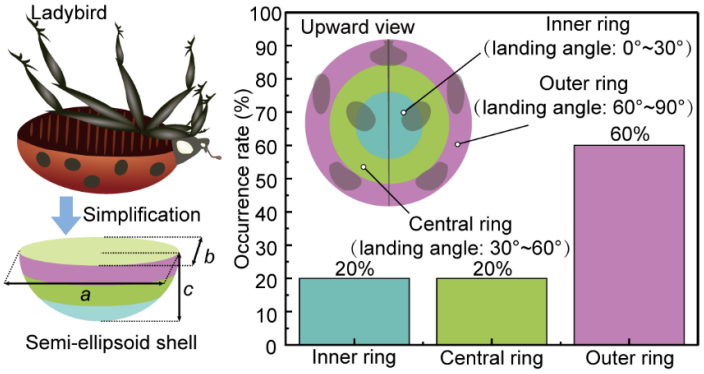

Figure 3. Diagram of impact regions. The inner ring, central ring, and outer ring on the elytra shell are shown in different colors. The probabilities of the ladybird landing on inner ring, central ring, and outer ring are 20%, 20%, and 60%, respectively.

After dropping 20 insects for 60 times, the probability of collisions in different regions of the elytra was measured to be 20%, 20%, and 60% for the inner, central, and outer rings, respectively (Supplementary Video S1). Figures 4a-4c show three typical landing orientations with the landing angles of 0°, 30°, and 60°. We also noticed that

the elytra may open up and split on account of impact during landing on the inner ring (figure 4(d)). To quantify the opening of the elytra after a collision, we measured the splitting angle, which was defined as the angle between the elytra. Consequently, we categorized the fall into four cases: landing with closed elytra with collision in the inner ring (case 1), central ring (case 2), and outer ring (case 3), and landing with elytra splitting with collision in the inner ring (case 4).

Figure 4. Snapshots of the falling insects. (a)-(c) Snapshots showing the different landing angles. (d) Snapshots showing elytra splitting under impact.

3.2. Kinematics of falls

To quantify the kinematics of falls, we measured the height, translational velocities and angular velocities of the ladybirds at 10 ms before and at 10 ms after collisions. For the cases in which the elytra showed no splitting (case 1-3), the heights were 29.17 ± 0.51 mm, 28.65 ± 0.72 mm, and 29.49 ± 0.56 mm, respectively (figure 5(a)), and the translational velocities were 2.79 ± 0.09 m/s, 2.59 ± 0.09 m/s, and 2.76 ± 0.04 m/s (figure 5(b)). Both heights and velocities vary only slightly, which indicates that kinematics of falls are almost consistent between case 1-3, prior to collisions. In contrast, we found that the heights and velocities in the rebound were noticeably different. The rebound height was smaller in larger landing angles. Specifically, the

rebound height of the ladybirds when they landed on the inner ring (landing angle: 0°-30°), was 15.41 ± 1.01 mm, which is only 3.08% of the initial height. This is about twice the rebound height of the ladybirds that landed on the outer ring (landing angle: 60°-90°). The translational velocity in the rebound also decreased from a peak value of 1.06 ± 0.08 m/s when the ladybirds landed on the inner ring to 0.31 ± 0.06 m/s when they landed on the outer ring. After landing, the ladybird bodies rapidly turned at an angular velocity of 540.87 ± 24.84 rad/s when they landed on the outer ring, whereas the angular velocities of the ladybirds landing on the central and inner rings were smaller and equal to 427.50 ± 14.72 rad/s, and 305.25 ± 29.02 rad/s, respectively. The observed rotations are likely due to the eccentric impact force generated at landing.

We found that the mechanical energy absorbed after landing were 68.46%, 57.46%, and 59.15% for collisions on the inner, central, and the outer rings, respectively. According to this, a ladybird landing on the inner ring is likely to absorb more impact energy than others (figure 5(c)). Moreover, force plate recorded the peak forces as 37.09 ± 1.51 mN, 30.23 ± 0.37 mN, and 17.29 ± 0.71 mN for impacts on the inner, central, and outer rings, respectively (figure 5(d)). Compared to landing on the outer ring, the peak impact force exerted on the inner ring was 214.52% larger. This inserts a force that is 14 times the ladybird body weight, and is likely to be the cause for the elytra splitting. However, interestingly, when splitting took place upon the collision, the rebound height, translational velocity, and angular velocity decreased to 9.09 ± 1.22 mm, 0.44 ± 0.02 m/s, and 139.50 ± 12.38 rad/s, respectively, compared to the closed elytra landing on the inner ring. Taking this into account, the energy absorption with the elytra splitting reached 93.16% of the initial mechanical energy. This suggests that the elytra splitting can dissipate the energy that could otherwise damage the ladybird body. The elytra splitting also reduced the impact force to 26.41 ± 1.76 mN, which is 71.21% of that generated in collisions when the elytra remain closed.

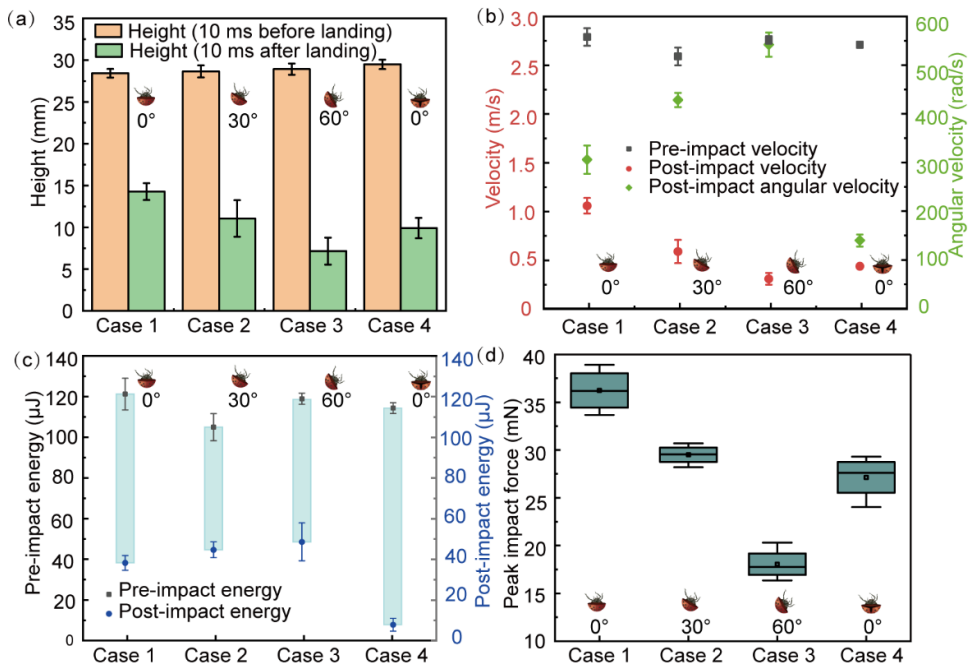

Figure 5. Kinematics of falls and impacts. (a) Height of the ladybirds from the ground. (b) Angular and translational velocities of the ladybirds before and after landing. (c) Energy absorption by the elytra during landing. (d) Peak impact force of the ladybird landing.

3.3. The role of the morphology and structure on the energy absorption in falls

To understand how the elytra splitting can increase the energy absorption in collisions, we developed a detailed model of the ladybird body, as shown in figure 6(a). The dome-like elytra are multi-layers structures, with an average thickness of 39.63 ± 1.01 μm. The elytra are coupled to each other by the tenon (35.89 ± 1.61 μm) that inserts into the mortise (33.84 ± 0.97 μm) (figure 6(b)).

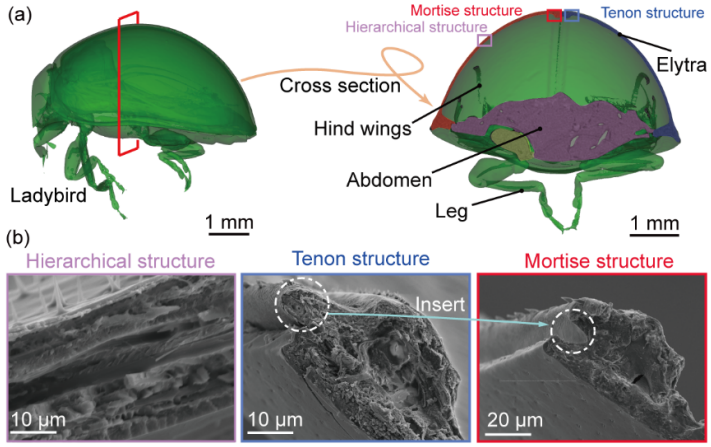

Figure 6. Morphology and microstructure of the ladybird elytra. (a) Micro-CT scans of a ladybird. (b) Scanning electron microscopy images of the elytra showing the structure of coupling.

Based on the geometry of the elytra, we proposed two comparative models to investigate the role of coupling in energy absorption during collisions, as shown in figure 7(a). A continuum model was presented as a quarter of a spherical shell with a radius R of 1.5 mm and a thickness d of 40 μm. In contrast to that, we also developed a split model that was identical to the continuum model, except that it was subdivided into two equally sized parts, which were connected using a coupling structure. The coupling structure was a simplified version of the real coupling, and had a semicircle cross section with a radius of 20 μm (figure 7(a)).

Here, we compared the mechanical response of the models at the landing angle of 0° (figure 7(b), Supplementary Video S2). The numerical simulation of collision includes three stages, as falling (1-2 in figure 7(b)), landing (2-3 in figure 7(b)), and rebound (3-4 in figure 7(b)). For the continuum model, the changes of internal energy can be subdivided into four phases (P_1-P_4 in figure 7(c)). Before the model contacts the ground, the internal energy of the model remains zero (P_1). During landing, the model deforms and the internal energy increases to 1.64 μJ (P_2). With the recovery of the elastic deformation, the model rebounds and its internal energy gradually declines to 0.07 μJ in P_3. Considering that the influences of the air resistance and structural damping were not considered in our simulations, in P_3, the model vibrates with a frequency of 7.48×10^5 rad/s.

The changes of the internal energy of the split model can be subdivided into five phases (Q_1-Q_5 in figure 7(c)). The internal energy of the split model in Q_1 and Q_2 are the same as those of the continuum model in P_1 and P_2, respectively, indicating that two models have the same state in these two phases. However, the split model experienced a larger deformation in phase Q_3, causing that the internal energy of the model to increase to 1.99 μJ. Hence, we suggest that the split model has an increased capacity to absorb energy, in comparison to the continuum model, because of splitting. Subsequently, with the release of elastic energy, the model also rebounds off the ground in phase Q_4, and vibrates with a frequency of 1.83×10^5 rad/s (Q_5). According to the free vibration frequency of the models after rebounding off the ground, we used the equation $K=\omega^2 m$ to measure the structural stiffness of the models. We discovered that

the stiffness of the continuum model is about 16.75 times that of the split model, which can explain the larger deformation of split model upon collision. A larger deformation induced by structural specificity, especially satisfying a range of specific physiological demands, can be found in other organs of insects, such as dragonfly wings (Rajabi *et al.*, 2015), and mosquito antennas (Saltin *et al.*, 2019).

The peak impact force of the split model is 66.67% of that of the continuum model (figure 7(d)). This means that elytra splitting can reduce the risk of damage in collisions. The increase in absorbed energy in the split model also reduces the rebound velocity (figure 7(e)). The rebound velocity of the split model is only half of that of the continuum model (1.35 m/s vs. 2.62m/s). This shows that the elytra splitting also reduces the kinetic energy of a falling ladybird during rebounding.

Besides its positive impacts, the elytra splitting may also have negative effects. The increased internal energy of the split model is accompanied by an increased level of stress within the model. As seen in figure 7(f), the peak average stress of the split model is 2.18 times that of the continuum model, which is caused by the comparatively larger deformation of the model. However, it seems that the stress developed within the split model is still too small to result in the failure of the material forming the elytra, which has a strength of about 72 MPa (Rajabi *et al.*, 2017).

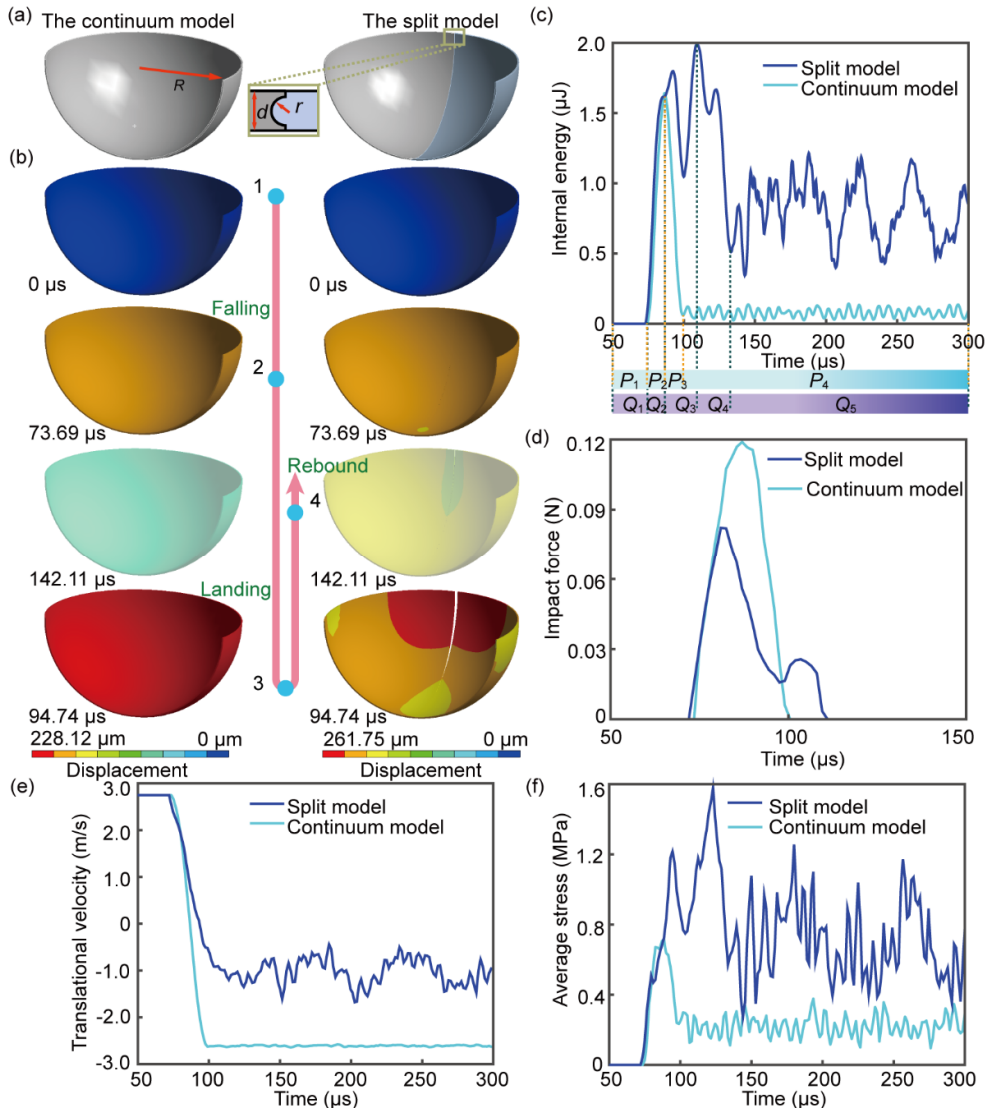

Figure 7. Numerical simulation of the mechanical behavior of the elytra in collisions. (a) The continuum and split models. *R*: radius of the spherical shell; *d*: the thickness of the shell; *r*: radius of the coupling. (b) Models reach the ground with a landing angle of 0°. Simulation of falls include three stages, as falling (1-2), landing (2-3), and rebound (3-4). (c) Comparison of the internal energy of the models. Falling of the continuum includes four phases. P_1: falling; P_2: elastic deformation during landing; P_3: shape recovery during rebound; P_4: free vibration. Falling of the split model includes five phases: Q_1: falling; Q_2: first elastic deformation during landing; Q_3: second elastic deformation during landing Q_4: shape recovery during rebound; Q_5: free vibration. (d)-(f) Comparison of the impact force, translational velocity and average stress of the models.

We further simulated the falls of the models with other landing angles (30° and 60°) (figures 8(a)-(b)). The split model always exhibited a higher energy absorption capacity, which reduced both the peak impact force (at least by 25.36%) and rebound velocity (at least by 3.40%), as shown in Table 2. The peak average stress of the split

model was at most 1.2 times larger than the other model. These results are consistent with those obtained from the simulation of falls at 0° landing angle (figures 7(c)-(f)). Additionally, we also found that with the increase of the landing angle, both the peak impact force and rebound velocity of the model reduced without absorbing more energy. This means that the risk damage can be reduced by simply adjusting the landing angles without absorbing more impact energy. This may explain why the ladybirds often landed on the outer ring, although it remains unclear whether this adjustment is done by means of active or passive mechanisms.

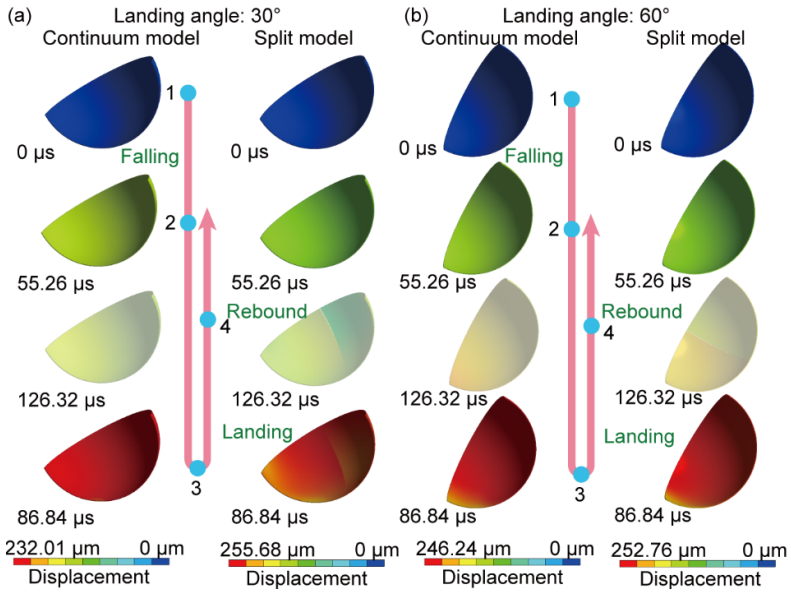

Figure 8. Numerical simulation of the falls in the landing angles of 30° and 60°.

Table 2. Numerical simulation results of the models

Model type	Landing angle (deg)	Internal energy (μJ)	Peak impact force (mN)	Rebound velocity (m/s)	Peak average stress (MPa)
Continuum model	30	1.13	73.71	2.47	0.69
	60	0.97	47.48	2.06	0.73
Split model	30	1.70	55.02	2.24	0.83
	60	1.63	41.09	1.99	0.77

3.4. Application

To demonstrate the application of the energy absorption mechanism discovered in this study, we fabricated the comparative models by 3D printing. We dropped the models from a height of 2 cm without initial velocity, and measured the impact forces

generated in collisions by a force plate (figure 9(a)). The short dropping distance of 2 cm enabled us to always have the landing angle of 0° in the experiments. The impact force of the continuum model is 1.72 ± 0.15 N, whereas that of the split model is 72.67% of the former (1.25 ± 0.10 N) (figure 9(b), Supplementary Video S3). To test the performance of the insect-inspired 3D printed models in real-world applications, we attached them as landers to the arms of a quadcopter (JY03, BBS, China) with a weight of ~0.2 kg (figure 9(c)). We let the quadcopter fly and then turned it off in a height of 26 cm above the ground to simulate a free-fall scenario (figures 9(d)-(e), Supplementary Video S4). The selected height was selected as it enabled us to capture the whole falling event within the frame of the camera. Similar to the results obtained from testing of isolated models, the peak impact force of the quadcopter equipped with 3D printed split models was smaller than, and only 74.85% of, that of the quadcopter equipped with 3D printed continuum models (figure 9(f)). The quadcopter equipped with 3D printed split models also experienced a smaller rebound height, in comparison to the quadcopter equipped with 3D printed continuum models (6.0 cm vs. 6.4 cm). As a result, it also became stable in a shorter time than the quadcopter equipped with 3D printed continuum models (1.14 s vs. 1.67 s).

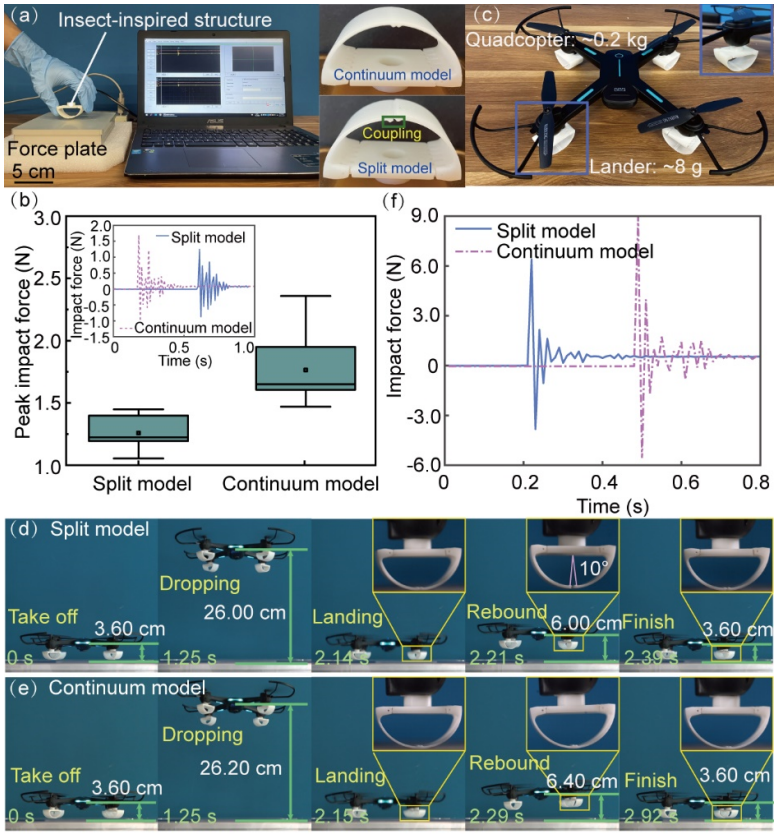

Figure 9. Insect-inspired 3D printed models in application. (a) Experimental setup. (b) The impact force of the split model (with coupling) and continuum model (without coupling) in falls. (c) A quadcopter equipped with four insect-inspired 3D printed models. (d)-(e) Comparison of the mechanical performance of the 3D printed split models and the 3D continuum models attached to the arms of a quadcopter. (f) Comparison of peak impact forces.

4. Conclusion

The results of our study suggest that elytra coupling may act as a mechanism to increase the energy absorption in intentional falls after encountering predators. This mechanism is achieved by the failure of the coupling upon excessive loads and may also exist in other beetle species. Three directions for future research seem particularly worth following. First, the intentional falls on the elytra may be achieved by the combined attitude regulation and in-flight maneuver (Zheng *et al.*, 2017), but there lacks extensive investigations on this problem. Second, comparative study of the mechanical behavior of the coupling mechanisms in insects that show a similar behavior can shed light on the diversity of this strategy. Third, detailed investigation of the specialized morphology and material properties of the coupling mechanism may inspire

the biomimetic design of insect-inspired energy absorption devices.

Competing interests

We declare we have no competing interests.

Funding

This work was supported by the National Natural Science Foundation of China (grant No. 51905556), the Grant for Popularization of Scientific and Technological Innovation of Guangdong Province (grant No. 2020A1414040007), and the research grant of Sun Yat-Sen University for Bairen Plan (grant No. 76200-18841223).

Acknowledgements

We thank Li Gong for the assistance in measuring the Young's modulus of elytra.

References

Behzad M, Hodaei M and Alimohammadi I 2007 Experimental and numerical investigation of the effect of a speed bump on car noise emission level *Applied acoustics* **68** 1346-56

Breed R S and Ball E F 1908 The interlocking mechanisms which are found in connection with the elytra of Coleoptera *The Biological Bulletin* **15** 289-303

Burgio G 2013 ECOLOGY AND BEHAVIOUR OF THE LADYBIRD BEETLES (COCCINELLIDAE) *European Journal of Entomology* **110** 94

Chen R-C, Dreossi D, Mancini L, Menk R, Rigon L, Xiao T-Q and Longo R 2012 PITRE: software for phase-sensitive X-ray image processing and tomography reconstruction *Journal of synchrotron radiation* **19** 836-45

Dai Z and Yang Z 2010 Macro-/micro-structures of elytra, mechanical properties of the biomaterial and the coupling strength between elytra in beetles *Journal of Bionic Engineering* **7** 6-12

Dai Z, Zhang Y, Liang X and Sun J 2008 Coupling between elytra of some beetles: mechanism, forces and effect of surface texture *Science in China Series C: Life Sciences* **51** 894-901

Drake A, Donahue T L H, Stansloski M, Fox K, Wheatley B B and Donahue S W 2016 Horn and horn core trabecular bone of bighorn sheep rams absorbs impact energy and reduces brain cavity accelerations during high impact ramming of the skull *Acta biomaterialia* **44** 41-50

Foelix R 2011 *Biology of spiders*: OUP USA)

Frantsevich L, Dai Z, Wang W Y and Zhang Y 2005 Geometry of elytra opening and closing in some beetles (Coleoptera, Polyphaga) *Journal of Experimental Biology* **208** 3145-58

Frazer B and Gilbert N 1976 Coccinellids and aphids *Journal of the Entomological Society of British Columbia* **73** 33-55

Full R J, Stokes D R, Ahn A N and Josephson R K 1998 Energy absorption during running by leg

muscles in a cockroach *Journal of Experimental Biology* **201** 997-1012

Fuller L H and Donahue S W 2021 Material properties of bighorn sheep (Ovis canadensis) horncore bone with implications for energy absorption during impacts *Journal of the Mechanical Behavior of Biomedical Materials* **114** 104224

Grunenfelder L, Suksangpanya N, Salinas C, Milliron G, Yaraghi N, Herrera S, Evans-Lutterodt K, Nutt S, Zavattieri P and Kisailus D 2014 Bio-inspired impact-resistant composites *Acta biomaterialia* **10** 3997-4008

Gunderson S and Schiavone R 1995 *Biomimetics: Design and Processing of Materials*: American Institute of Physics Woodbury) pp 163-97

Hadley N F 1986 The arthropod cuticle *Scientific American* **255** 104-13

Hao P and Du J 2018 Energy absorption characteristics of bio-inspired honeycomb column thin-walled structure under impact loading *Journal of the mechanical behavior of biomedical materials* **79** 301-8

Hien T and Kleiber M 1990 Finite element analysis based on stochastic Hamilton variational principle *Computers & structures* **37** 893-902

Hong C, Maosheng C and Jiurong S 2003 Histological structures of the dung beetle, Copris ochus Motschulsky integument *Kun Chong xue bao. Acta Entomologica Sinica* **46** 429-35

Jalali S and Heshmati M 2016 Buckling analysis of circular sandwich plates with tapered cores and functionally graded carbon nanotubes-reinforced composite face sheets *Thin-Walled Structures* **100** 14-24

Kundanati L, Signetti S, Gupta H S, Menegon M and Pugno N M 2018 Multilayer stag beetle elytra perform better under external loading via non-symmetric bending properties *Journal of The Royal Society Interface* **15** 20180427

Lee N, Horstemeyer M, Rhee H, Nabors B, Liao J and Williams L N 2014 Hierarchical multiscale structure–property relationships of the red-bellied woodpecker (Melanerpes carolinus) beak *Journal of The Royal Society Interface* **11** 20140274

Li M, Xi N, Wang Y and Liu L 2019 Tunable hybrid biopolymeric hydrogel scaffolds based on atomic force microscopy characterizations for tissue engineering *IEEE transactions on nanobioscience* **18** 597-610

May P R, Fuster J M, Haber J and Hirschman A 1979 Woodpecker drilling behavior: an endorsement of the rotational theory of impact brain injury *Archives of Neurology* **36** 370-3

Phan H V and Park H C 2020 Mechanisms of collision recovery in flying beetles and flapping-wing robots *Science* **370** 1214-9

Rajabi H, Ghoroubi N, Darvizeh A, Dirks J-H, Appel E and Gorb S N 2015 A comparative study of the effects of vein-joints on the mechanical behaviour of insect wings: I. Single joints *Bioinspiration & biomimetics* **10** 056003

Rajabi H, Jafarpour M, Darvizeh A, Dirks J-H and Gorb S 2017 Stiffness distribution in insect cuticle: a continuous or a discontinuous profile? *Journal of The Royal Society Interface* **14** 20170310

Rhee H, Horstemeyer M, Hwang Y, Lim H, El Kadiri H and Trim W 2009 A study on the structure and mechanical behavior of the Terrapene carolina carapace: a pathway to design bio-inspired synthetic composites *Materials Science and Engineering: C* **29** 2333-9

Rivera J, Hosseini M S, Restrepo D, Murata S, Vasile D, Parkinson D Y, Barnard H S, Arakaki A, Zavattieri P and Kisailus D 2020 Toughening mechanisms of the elytra of the diabolical

ironclad beetle *Nature* **586** 543-8

Saltin B, Matsumura Y, Reid A, Windmill J, Gorb S and Jackson J 2019 Material stiffness variation in mosquito antennae *Journal of the Royal Society Interface* **16** 20190049

Sensenig A T, Lorentz K A, Kelly S P and Blackledge T A 2012 Spider orb webs rely on radial threads to absorb prey kinetic energy *Journal of The Royal Society Interface* **9** 1880-91

Shang Z, Li T, Yang S, Yan J and Guo H 2020 Three-dimensional characterization of typical inclusions in steel by X-ray Micro-CT *Journal of Materials Research and Technology* **9** 3686-98

Sun J and Bhushan B 2012 Structure and mechanical properties of beetle wings: a review *Rsc Advances* **2** 12606-23

Tarakanova A and Buehler M J 2012 The role of capture spiral silk properties in the diversification of orb webs *Journal of the Royal Society Interface* **9** 3240-8

Tasdemirci A, Kara A, Turan K and Sahin S 2015 Dynamic crushing and energy absorption of sandwich structures with combined geometry shell cores *Thin-Walled Structures* **91** 116-28

Trim M W, Horstemeyer M, Rhee H, El Kadiri H, Williams L N, Liao J, Walters K B, McKittrick J and Park S-J 2011 The effects of water and microstructure on the mechanical properties of bighorn sheep (Ovis canadensis) horn keratin *Acta biomaterialia* **7** 1228-40

Wang Z, Zhang W, Wu J and Yang Y 2020 An Approach to Observing and Quantifying Real-Time Mandibular Muscle Topology in the Trap-Jaw Ant Odontomachus monticola by Synchrotron Imaging *Journal of Insect Behavior* **33** 174-83

Wu Y, Liu Q, Fu J, Li Q and Hui D 2017 Dynamic crash responses of bio-inspired aluminum honeycomb sandwich structures with CFRP panels *Composites Part B: Engineering* **121** 122-33

Xie H-L, Deng B, Du G-H, Fu Y-N, Guo H, Xue Y-L, Peng G-Y, Tao F, Zhang L and Xiao T-Q 2020 Methodology development and application of X-ray imaging beamline at SSRF *Nuclear Science and Techniques* **31** 1-21

Zhang J, Li J, Li C, Wu Z, Liang H and Wu J 2021 Self-righting physiology of the ladybird beetle Coccinella septempunctata on surfaces with variable roughness *Journal of Insect Physiology* 104202

Zheng X, Wang C, Fan R and Xie G 2017 Artificial lateral line based local sensing between two adjacent robotic fish *Bioinspiration & biomimetics* **13** 016002